J. Min. Metall. Sect. B-Metall., 56 (3) (2020) 289 - 297

Journal of Mining and Metallurgy,
Section B: Metallurgy

DETERMINATION OF METALLIZATION DEGREE OF PRE-REDUCED CHROMITE WITH IMAGE AND RIETVELD ANALYSIS

T. Leino [a], P. Taskinen [a,*], R. H. Eric [a, b]

[a] Department of Chemical and Metallurgical Engineering, Aalto University, Aalto, Finland
[b] School of Chemical and Metallurgical Engineering, University of the Witwatersrand, South Africa

(Received 24 September 2019; accepted 12 May 2020)

Abstract

Metallization degree of pre-reduced chromite was determined using two methods. The chromite samples were reduced in the solid state by methane-hydrogen gas mixtures. First method was image analysis of micrographs obtained by scanning electron microscope where heavier metallic phases appeared as bright white areas which were relatively easy to segment using a thresholding algorithm. The second technique was Rietveld analysis of X-ray powder diffraction pattern which fitted a calculated profile onto a measured X-ray diffraction pattern to gain information about phase quantities. Rietveld refinement and phase composition analysis was performed with PANalytical's X'Pert HighScore Plus software from the XRPD (X-ray powder diffraction) data. Both techniques were in good agreement. Metallization degrees for the investigated samples ranged from 15 to 65 % depending on the extent of reduction which was a function of time, reduction temperature, and methane content of the gas mixture. These results were promising and indicate that either image analysis or X-ray Rietveld analysis can be used as a relatively fast method to determine the degree of metallization of pre-reduced samples in comparison to the slow and tedious chemical analysis.

Keywords*: Ferrous chromite, Metallization, Image analysis, Rietveld analysis*

1. Introduction

The pre-reduction of ferrous chromite brings advantages in the ferrochromium production when most chemical work can be accomplished at lower temperatures than smelting and only the final phase separation is then carried out at typical smelting temperatures [1]. The reaction paths of chromite with methane are complicated due to the formation of carbides at relatively low temperatures [2, 3]. This conveys difficulties in the analysis of reduction products and, thus, reduction or metallization kinetics is accompanied with carbide formation, cracking of the excess methane, and soot formation on the surfaces of the reacting samples [4].

The aim of this work was to determine how much metal, whether pure or as carbide, was yielded by the methane prereduction performed on Kemi Chromite ore from Finland. Two different analysis methods were used: image analysis of scanning electron microscope (SEM) micrographs and Rietveld analysis of X-ray powder diffraction (XRPD) patterns. The experimental research and the obtained results were done within the Master's thesis of T. Leino [5].

2. Image analysis (SEM)

The first step in image analysis is to divide an image into meaningful regions which could be used for further analysis. One of the simplest segmentation methods is thresholding which transforms an image f(x, y) to a binary image g(x, y) by choosing a threshold value T.

$$g(x,y)=\begin{Bmatrix}1,\ if\ f(x,y)\geq T\\ 0,\ otherwise\end{Bmatrix} \quad (1)$$

Each pixel (x, y) is separated into one of two classes: object and background points. If the pixel intensity value is greater than the threshold T, it is an object point, otherwise it is a background point [6]. In Fig. 1, a SEM electron micrograph of reduced chromite was thresholded using two different values. The intensity histogram of the original image showed the number of pixels at each intensity value. The intensity values went from 0 (black) to 255 (white). Using a thresholding value of 30 effectively selected all but the darkest pixels. In order to select only the brightest pixels, a higher thresholding value, such as 240, had to be selected.

*Corresponding author: pekka.taskinen@aalto.fi

https://doi.org/10.2298/JMMB200313022L

A suitable threshold value can be chosen by evaluating the image by eye while changing the threshold value. However, this manual way quickly becomes tedious when processing large amounts of images and the attained results may not be reproducible. For this reason, thresholding is usually automated by using an algorithm. There are several types of thresholding methods [7], but in this work the focus was on the histogram shape-based methods which analyze, for example, the peaks and valleys of the histogram. The algorithms discussed next are global thresholding techniques which means the thresholding value was held constant throughout the image.

Otsu's Method

The idea behind the Otsu's method [8] is to find the threshold that minimizes the within-class variance. This method assumes that the histogram is bimodal (has two maxima) and the valley between these two peaks is deep and sharp. Also, illumination must be uniform so only the object appearance differences cause the brightness behavior [9]. The gray-level histogram h(i) of the examined image was first normalized and treated as a probability distribution.

$$h(i) = n_i / N_P, \quad h(i) \geq 0, \quad \sum_{i=1}^{L} h(i) = 1 \tag{2}$$

where N_p is the number of pixels in the image, n_i is the amount of pixels at intensity level i, and L is the total number of possible intensity levels in the image (i.e., 256 for an 8-bit gray-level image). The following step was to split up pixels in the image into two classes, C_0 and C_1 (i.e., background and objects, respectively) by a threshold value T. So, where C_0 denotes pixels with intensity levels [0, · · · , T −1] and C_1 refers to pixels with levels [T, · · · ,L−1]. The occurrence probabilities for these classes were calculated as follows:

$$P_r(C_0) = \sum_{i=1}^{T} h(i) \tag{3}$$

$$P_r(C_1) = \sum_{i=T+1}^{L} h(i) \tag{4}$$

Then the mean intensity and class variance values were evaluated statistically and from these through iteration of all the probable threshold levels T (from 0 to 255 for an 8-bit image). The one that yields the lowest class variance value was chosen as the threshold.

Huang's Method

Huang's method [10] utilizes fuzzy logic for selecting the optimal threshold. In contrast to Boolean logic where the variable values can be either 0 or 1, fuzzy logic allows variables to be any real number between 0 and 1. This is beneficial when selecting a

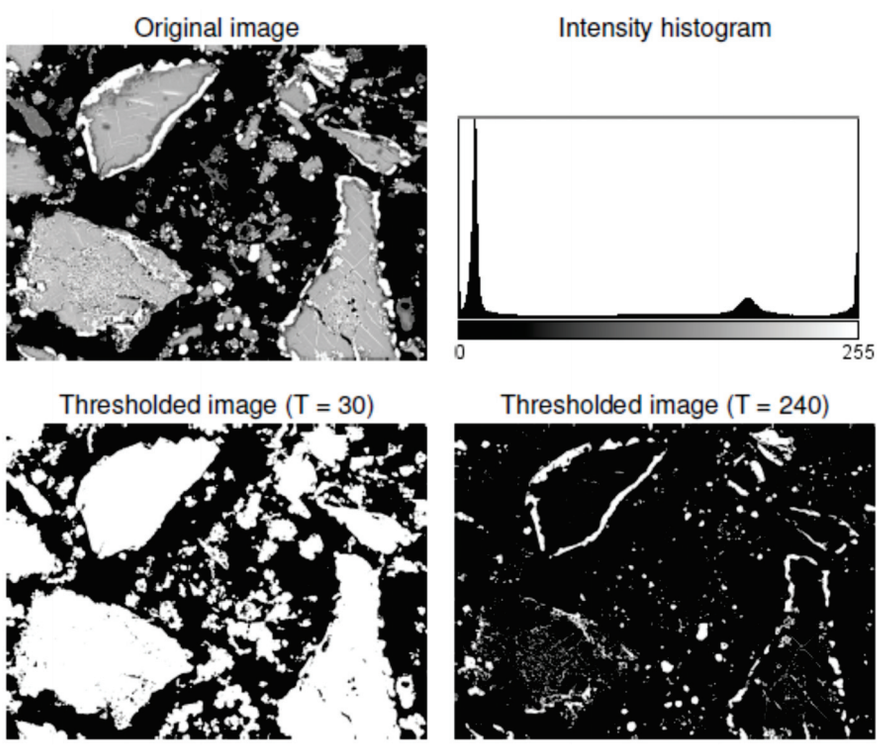

Figure 1. *Thresholding the original electron image with a value of 30 basically includes all but the darkest pixels, while a thresholding value of 240 only selects the brightest pixels as object points and marks the rest as background points*

threshold because class probability densities often overlap due to ambiguous data. Fuzzy logic deals with fuzzy sets whose elements have degrees of membership described with the aid of a membership function. In effect, this means that one element can be part of multiple sets. In case of selecting a threshold, a fuzzy set (an image) was considered as an array of fuzzy singletons (image pixels). Each of them has a membership value associated with the intensity level of the pixel. Image I could then be represented as:

$$I = \left\{ f(x,y), \mu_I \left(f(x,y) \right) \right\} \quad (5)$$

where μ_I is the membership function. In this method, the normalized histogram h(i), which groups all pixels f(x, y) having the same intensity/gray levels i, was utilized to calculate the membership function together with mean intensity values/levels with statistical procedures which is rather complex and beyond the scope of this paper and hence will not be illustrated here. The calculation procedure eventually provided the chosen threshold value.

Rietveld analysis

In order to get information about the crystal or chemical structure of a sample, it was necessary to build a mathematical diffraction pattern and compare it to the measured one. Integrated intensity I_{hkl} for each hkl (representing the crystallographic plane indices) reflection can be calculated with Eq. (6):

$$I_{hkl} = \left(F_{hkl} \right)^2 \cdot LP_{hkl} \cdot P_{hkl} \cdot A \cdot E_{hkl} \quad (6)$$

where F_{hkl} is the structure factor, LP_{hkl} is the Lorentz-polarization factor, A is the absorption factor, P_{hkl} is the preferred orientation factor, and E_{hkl} is the extinction factor [11]. The explanation and mathematical description of all the factors mentioned above is again complex and beyond the scope of this paper and can be found elsewhere [5]. The integrated intensity equation gives a single intensity value for a single 2Θ angle. This value is used to represent the area under a real X-ray diffraction peak. The Rietveld method distributes this single value across a range of 2Θ angles creating a peak profile similar to the observed one. The aim is to minimize the difference between the calculated and observed peak profiles by using the method of least-squares. A simple and widely used way of fitting the background is to use a polynomial function in 2Θ. Typically, Rietveld programs use a 5th degree polynomial. Refinement of only three of the five coefficients are enough to achieve a good background fit. All five coefficients are needed only for more complex backgrounds. For very complex backgrounds, also specific background formulas are available [12]. In order to place the calculated profile of each phase onto the same scale as the measured one, a scale factor is employed. Shape of the measured profile peak depends on various aspects such as the characteristics of the incident beam, experimental arrangements, diffractometer, sample size and shape [13, 14]. Various peak shape functions have been used to approximate these effects. In his original paper, Rietveld [15] used a Gaussian profile for the peak shape.

The Rietveld refinement method uses fitting parameters which are divided into two groups: global and phase-dependent. Global parameters include e.g. the machine zero offset, specimen displacement, and pattern background and are, for the most part, phase-independent. Phase-dependent parameters include phase spike widths, unit scale dimensions and so on. Some of these phase-dependent parameters are stable, but most are unstable. An effective refinement strategy involves a step-by-step parameter turn-on sequence where only the stable parameters are refined first and additional parameters are turned on for the following cycles [16]. This kind of systematic approach aims at preventing situations where a premature refinement of non-linear and very unstable parameters leads to erratic behavior or to failure of the whole refinement. When parameters are turned on one by one, it is also easier to spot a troublemaking parameter if the refinement is not progressing smoothly.

In this work, the Rietveld refinement and phase composition analysis was performed with an available PANalytical's X'Pert HighScore Plus program from the XRPD data. It utilizes all the principles mentioned above.

2. Research Methods

Image analysis was performed on the SEM micrographs taken from Leikola's [17] samples in addition to those of the newly prepared and reduced samples. Each new sample was prepared from approximately five grams of chromite concentrate (from Kemi, Finland) reduced for 60 minutes at temperatures and CH_4-H_2 atmospheres shown in Table 1. Additionally, three E series of experiments (E04, E10, and E16) were also performed at 1350 ºC with 30% methane in the gas mixture and a duration of 75, 90, and 120 minutes. To decrease the particle size and ensure a uniform size distribution, each sample was ground with the Retsch XRD-Mill McCrone for 10 minutes. Size distribution of each ground sample was examined with Malvern Instruments Mastersizer 2000. After the XRPD measurements, the powders were cast into epoxy and wet ground with silicon carbide papers and polished with 3 and 1 μm monocrystalline diamonds. In order to increase the conductivity and get better image quality in SEM, the polished samples were carbon coated with a Leica EM SCD050 cool sputtering device. The Rietveld analysis

on E series samples (see Table 2) were rather erratic due to extensive carbon precipitation and hence were abandoned.

The gas components used in the experiments were argon (Ar, 99.999 vol%), methane (CH_4, 99.5 %), and hydrogen (H_2, 99.99 %) from Aga-Linde. The total gas flow was kept at 800 mL/min during the experiments. A closed electrical, horizontal tube furnace was utilized to conduct the experiments. SEM micrographs were taken with a LEO model 1450 VP (Carl Zeiss, Germany) using Oxford Instruments INCA software at x1500 magnification. A total approximately 25 images were taken for each sample.

The SEM micrographs had four distinctive phases in addition to the black epoxy. Leikola's study [17] confirmed this, where used samples, examined using energy dispersive X-ray spectroscopy (EDS), showed the phases to be silicate (very dark gray), two kinds of chromite (dark-partially reduced and light gray-unreduced), and metal/metal carbide (white). These phases are marked in Figure 2. MATLAB (R2016a) with the Image Processing Toolbox (version 9.4) was used to perform the image analysis.

First, Otsu's method [8] was used to calculate three threshold levels for the SEM micrograph to separate the phases. This caused the last threshold level to include some brighter but gray areas in addition to totally white ones. Thus, this last threshold section was thresholded again. This additional thresholding was done with the Otsu's method [8] but for some images the approach was too generous, i.e. it still caused some light gray areas to remain. Huang's method [10] was found to be more suitable for the images in question and was thus used to further segment the brightest phases.

Table 1. *Experimental temperatures and atmospheres employed for each sample*

Sample	T [°C]	CH_4		H_2	
		[vol %]	[ml/min]	[vol %]	[ml/min]
A04	1100	10	80	90	720
A10	1100	20	160	80	640
A16	1100	30	240	70	560
B04	1200	10	80	90	720
B10	1200	20	160	80	640
B16	1200	30	240	70	560
C04	1300	10	80	90	720
C10	1300	20	160	80	640
C16	1300	30	240	70	560
D04	1350	10	80	90	720
D10	1350	20	160	80	640
D16	1350	30	240	70	560

Figure 3 shows the original SEM micrograph and an image where the brightest threshold level was colored in green and placed on top of the original image for comparison. As one can see, the thresholding method finds the brightest metal phase with good accuracy.

Next, the original image was separated into binary sub images according to the calculated threshold levels. This way, each phase had its own sub image where a white pixel indicated the phase was present and a black pixel that it was absent.

To exclude the black epoxy from the calculations, area fraction Af was calculated for each phase by dividing the area of the phase with area of all phases. This area percentage was then converted to mass percentage Mp by multiplying with density of the phase in question: The brightest phase was found, in the Rietveld analysis, to consist mostly of iron and chromium carbide so a density of 7.8 g/cm^3 was used for it [18]. A density of 4.8 g/cm^3 was used for the two chromite phases and a density of 2.0 g/cm^3 for the darkest phase of various silicates.

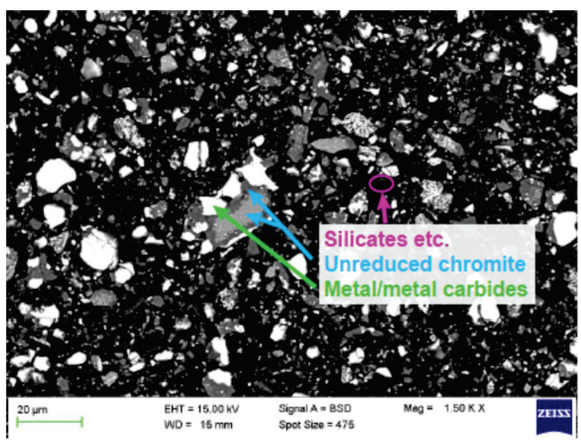

Figure 2. *Different phases found in the sample; the bright white phases are metal alloy or metal carbides, the darker and lighter gray are unreduced chromite and the very dark gray includes silicates*

All density values were given by PANalytical's X'Pert HighScore Plus program (version 4.0). Finally, the mass percentages were normalized. Even though the mass percentages were calculated for all of the phases, only the most interesting metal phase was analyzed and discussed.

XRPD measurements were conducted with PANalytical's X'pert3 Powder X-ray diffraction system using Cu Kα radiation. Samples were backloaded into a spinning sample holder. The qualitative analyses were conducted with the PANalytical's X'Pert HighScore Plus program (version 4.0). The program rated different minerals based on how well they fitted on the XRD pattern.

The likely minerals contained by the sample were chosen with the help of the score given by the program and our prior knowledge of the sample and reduction process. The quantitative Rietveld analyses were also performed with the same software, using refinement steps as suggested by Taylor [12] and Young [16].

3. Results and discussion

The results from the image and Rietveld analyses are presented and discussed here. It is evident from experiments that the metal alloy content of the partially reduced samples increased with increasing reduction temperature. The CH_4 content or the reduction time did not seem to play a major role at the lower reduction temperatures. At higher temperatures, the methane content had a much more significant role especially when the reduction time was short. Image analyses were also performed in this study on Leikola's [17] samples which were already mounted and polished. Table 2 compares the metal contents between the image analysis performed on Leikola's samples and samples from this work for experiments performed under similar conditions. Leikola's samples had higher metal content across the board but the difference was not significant. The difference may be due to the small amount of Leikola's samples (1g compared to 5 g samples of this work) used in the experiments.

The percent metallization values determined by chemical methods on Leikola's samples were also in good agreement with the values reported in Table 2. The standard deviations as a percentage of all the samples in Table 2 were in the 0.22 % to 1.66 % range.

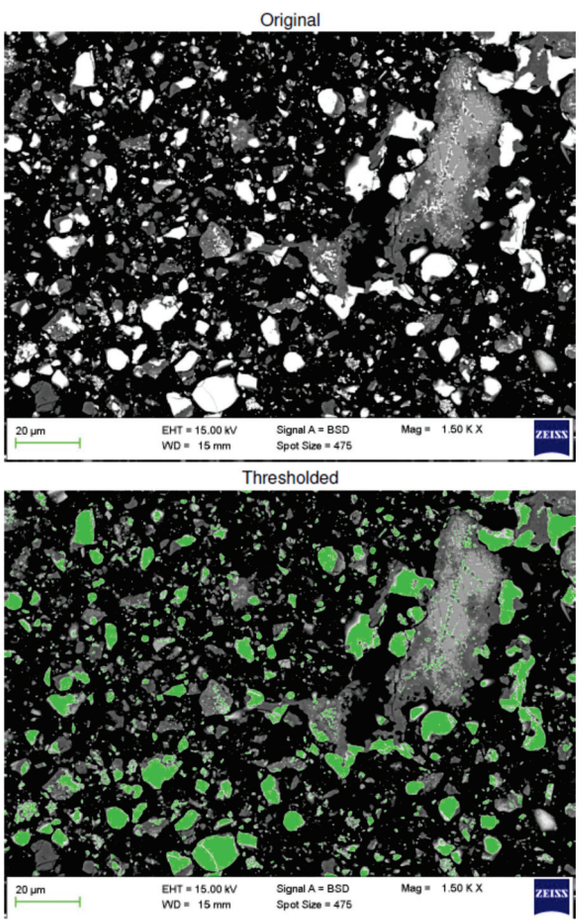

Figure 3. *Original SEM micrograph and an image, where the brightest threshold level was calculated with the present algorithm, colored green and superimposed on the original image*

Table 2. *Results on image analysis and Rietveld analysis for the metal content (% metallization) of reduced samples from Leikola's work [17] and this work; results from E series experiments were only from this work conducted at 1350 °C with 30 vol% methane for 75 (E04), 90 (E10) and 120 (E16) minutes*

Sample	Leikola samples (image analysis) wt% metal	This work (image analysis) wt% metal	This work (Rietveld analysis) wt% metal
A04	22.91	20.14	19.27
A10	20.93	19.21	20.34
A16	21.41	18.17	17.86
B04	32.9	31.96	32.11
B10	35.79	34.92	36.04
B16	28.91	27.76	29.91
C04	47.3	46.91	45.63
C10	46.52	45.86	43.92
C16	48.28	47.89	46.11
D04	51.75	50.81	48.24
D10	58.17	58.01	57.51
D16	18.65*	66.09	65.43
E04	-	72.61	**
E10	-	76.86	**
E16	-	83.62	**

Figure 4 shows an XRD pattern of sample B16 with the major peaks labelled. As can be seen, most of the peaks belonged to the three major phases: chromite, chromium carbide, and spinel. The carbon peak around 2q = 26º included at least two different carbon phases identified to be graphite 2H and graphite 3R. The range 43º - 46º also included other phases, such as iron and iron carbide, buried under the chromite and chromium carbide peaks. Due to severe overlapping of the peaks, especially at around 43º -

46º, some phases were likely missed during the qualitative analysis. Thus, an additional and more accurate analysis would have been beneficial to identify these minor phases which would have increased the accuracy of the Rietveld refinement.

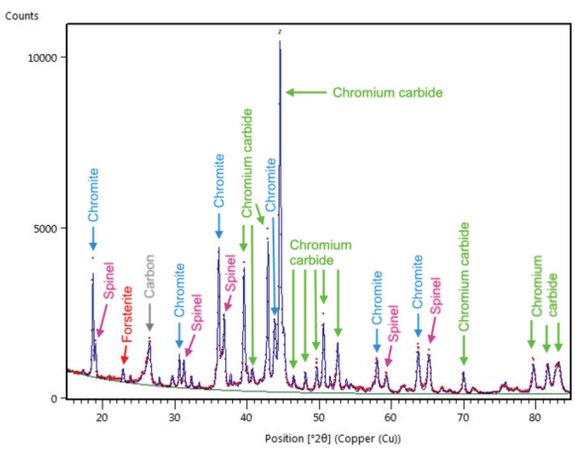

Figure 4. *XRD pattern of the sample B16 where the major peaks were labeled*

The results from Rietveld analysis for the samples of this work are also presented in Table 2. Figure 5 illustrates the results of Rietveld procedure in a column graph. It must be noted that the carbon, mineral, chromite, and carbide/metal content graphs combine the corresponding phases of all the graphite, the non-reducible oxide phases like magnesium-aluminium spinels, as yet unreduced chromite and all the metallic phases including all the carbides, respectively.

Carbon content was around 25–35 wt % in the A and B sets where the fraction of methane did not seem to affect the carbon deposition. In the higher temperature experiments (C and D sets) the carbon content was highly affected by the experiment atmosphere but the amount of carbon remained more or less the same as in the A and B sets or even lower. An exception was sample C16 which had a much higher carbon level, probably due to the high level of CH_4 (30 vol%) in the gas. It is also possible that i) the carbon deposited on walls of the furnace tube or the outer surface of the crucible at the higher temperatures or ii) reduction process consumed more carbon as the temperature rose and thus the carbon content was lower. However, carbon content of the E-series samples (where the reduction periods were longer and gas phase contained 30 % CH_4 at the highest temperature of 1350 ºC) was very high, and well above 60 % and suppressed the peaks of the other constituents in such a way that reliable and consistent results could not be obtained.

Chromite content decreased as the reduction temperature increased as expected, with exception of the samples D04 and D10, which were not in accordance with the increasing carbide/metal contents as well. This may be due to peak overlaps. Mineral content was not affected by the experimental parameters and remained more or less the same across

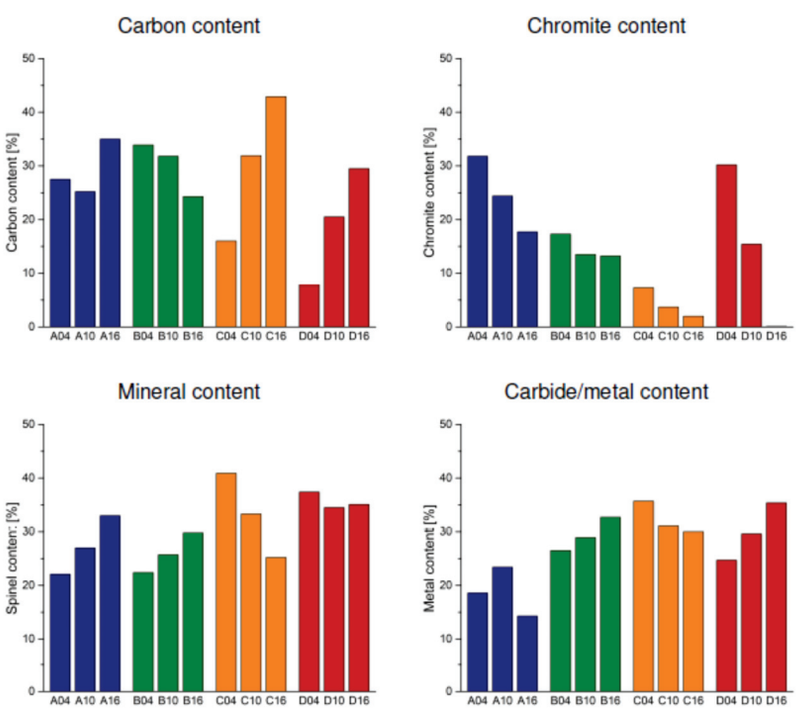

Figure 5. *Carbon, chromite, spinel, and metal contents as obtained by the Rietveld analysis*

all samples. The carbide/metal contents followed the same trends with the image analysis results for this work's samples.

For calculation purposes, when necessary (i.e. when the total analysis deviated from 100 %), the percentage of carbon, chromite, mineral, and carbide/metal content values directly from the Rietveld analysis were first normalized to 100 %. This procedure slightly changed percentages of the reported phases. Then the normalized carbon percentage was subtracted from 100 % and the total of the values of the three remaining phases were again normalized to 100 %. The subtraction of carbon values was due to the fact that carbon had precipitated directly from the gas phase and was not a constituent of the reduced chromite. Thus, the total content of three phases; chromite, mineral, and carbide/metal added up to 100 %. The new normalized values for the metal phase now represented the fractions of metallization of the reduced chromite sample. Percent metal values in Table 2 for the Rietveld analysis were calculated by this procedure. A comparison of the percent metal values in Table 2 from the image and the Rietveld analysis clearly showed that the agreement between the two sets of results was excellent.

The chemical analysis was performed on samples A10, B10, C10, and D10 from Table 2 yielding the following metallization degrees:

A10: 20.1 %, B10: 36.0 %, C10: 45.9 %, and D10: 58.0 %.

These numbers represented total metallization in terms of Fe and Cr contents and defined as following:

M_i (metallization of species i ≡
(% of metallized i in the sample by
chemical analysis) / (total % of i
in the sample from ore composition). (7)

Obviously, these metallization degree percentages are slightly different than the total metal % values from the image analysis and Rietveld analysis as they determine the metal phase percentage over the whole sample. The agreement is excellent proving the fact that both of the new techniques can give very good and representative results if done properly.

4. Summary and conclusions

The aim of this work was to determine the metal content of reduced chromite concentrate samples using image analysis and Rietveld analysis. The samples produced by Leikola [17] were used as a basis for image analysis but also for the XRDP measurements, new experiments were conducted with the same parameters used in Leikola's study. The four reduction temperatures used were 1100ºC (A-set), 1200ºC (B-set), 1300ºC (C-set), and 1350ºC (D and E-sets) and the three methane contents used were 10, 20, and 30 volume percent with hydrogen gas as the balance. The reduction period for the A-, B-, C-, and D-sets was chosen as 60 minutes. The E-set was conducted at 1350ºC using 30% CH_4 in the gas phase for the duration of 75, 90, and 120 minutes.

The image analyses were conducted from SEM electron micrographs using a thresholding algorithm written in MATLAB. Four phases were separated from the micrographs and for each phase a normalized weight percentage concentration was calculated. Only the metallized phase consisting of metal alloys and carbides was of interest in this work for the pre-reduction of chromite concentrate. For all the samples, the metal content was found to steadily increase with higher temperature, longer reduction period, and increasing CH_4 content in the gas. Results for the samples produced in this work were slightly lower than Leikola's samples [17]. The likely causes for the different metal contents were i) smaller particle size used in the study, which created a more uniform phase distribution and prevented formation of large metal particles that had the tendency of dominating the analysis and ii) a larger sample size used in this work which may have slowed the reduction process. Overall, image analysis worked well for the samples in question. The bright metal phase was easy to segment from the other phases. In addition, hundreds of SEM micrographs were quickly analyzed with the algorithm. However, since the bright areas of the SEM micrographs included all the heavier metallic phases, they were always analyzed as one composite phase without an option for a more detailed examination.

Rietveld refinement and the phase composition analysis were performed with PANalytical's X'Pert HighScore Plus program from the XRPD data. Metal content results from the Rietveld analysis were quite close to those obtained from image analysis. However, a more accurate knowledge of the mineral composition would have likely increased the quality of the results gained from the Rietveld analysis. Another factor was the low number of parameters refined for the minor phases in this study, in order to keep the refinement stable. Altogether, the Rietveld refinement is an effective and quantitative method but requires an experienced user. One has to know precisely the chemical and mineral composition of the studied mineral sample, with experience to obtain good XRPD measurements, and have extensive knowledge of the mathematics utilized to determine whether the obtained results are feasible. Also, a high number of substances and impurities in this kind of mineralogical samples complicate the procedure and make it more time consuming.

The metallization degree results for these

laboratory scale experiments were promising. Improvements for the subsequent image analyses would include automation of the SEM imaging process to increase the number of images to be analyzed. This way the whole sample could be scanned, thus reducing the chance that one highly reduced or non-reduced random area dominates the analysis. If the Rietveld method is used, the chemical and mineralogical compositions of the mineral samples need to be known accurately. Also, the analyses should be performed by an experienced operator.

We would consider image analysis to be somewhat more reliable than the Rietveld method provided that a significant number of representative electron images are scanned. This is due to the fact that it is a more direct method, looking to the metallized and unmetallized regions on the samples all of which are already visible.

Acknowledgements

The authors are grateful to Tekes and Academy of Finland for providing the part-time Finland Distinguished Professor position to R. H. Eric and funds for this research project. The authors will acknowledge that this paper was partly presented at INFACON XV: International Ferro-Alloys Congress held in Cape Town, South Africa on February 25-28, 2018 and is published with the permission of the Southern African Institute of Mining and Metallurgy who published this paper in the conference proceedings.

References

[1] E.L.J. Kleynhans, J.P. Beukes, P.G. van Zyl, J.R. Bunt, N.S.B. Nkosi, M. Venter, Metal. Mater. Trans. B, 48B (2) (2017) 827-840.

[2] N.M. Anacleto, I. Solheim, B. Sørensen, E. Ringdalen, O. Ostrovski, INFACON XV International Ferro-Alloys Congress (Eds. R.T. Jones, P. den Hoed, M.W. Erwee). SA IMM, Cape Town, 2018, p. 71-78.

[3] M. De Campos, H.H. Eric, Sohn Internat. Symposium, Vol. 1 (Eds. F. Kongoli & R. Reddy). TMS, Warrendale (PA), 2006, p. 613-621.

[4] V. Canaguier, L. Kolbeinsen, Extraction 2018 (Edits. B.R. Davis, Moats M.S. & Wang S.). TMS, Warrendale (PA), 2018, p. 1141-1152.

[5] T. Leino, Determination of Metallization Degree of Pre-reduced Chromite with Image and Rietveld Analysis. Master's Thesis, Aalto University, School of Chemical Technology, Espoo, 2017.

[6] R.C. Gonzalez, R.E. Woods, S.L. Eddins, Digital image processing using MATLAB. 1st Ed. Prentice Hall, New Jersey (USA), 2004.

[7] M.Sezgin, B. Sankur, Journal of Electronic Imaging, 13 (1) (2004) 146–165.

[8] N. Otsu, IEEE Transactions on Systems, Man and Cybernetics, 9(1) (1979) 62–66.

[9] J. Kittler, J. Illingworth, IEEE Transactions on Systems, Man and Cybernetics, 15 (5) (1985) 652–655.

[10] L-K. Huang, M-J. J. Wang, Pattern Recognition. 28 (1) (1995) p. 41–41.

[11] B.D. Cullity, Elements of X-ray Diffraction. 2nd Ed. Addison-Wesley Publishing Company, Massachusetts (USA), 1978.

[12] J.C. Taylor, I. Hinczak, Rietveld Made Easy: A Practical Guide to the Understanding of the Method and Successful Phase Quantifications. 4th Ed. Sietronics Pty Ltd. Canberra (Australia), 2006.

[13] R. Delhez, Crystal Imperfection Broadening and Peak Shape in the Rietveld Method. In: Young, R. A. The Rietveld Method. 1st Ed. Oxford University Press, Oxford (UK), 1992, p. 132–166.

[14] P. Suortti, Bragg Reflection Profile Shape in X-ray Powder Diffraction Patterns. In: Young, R. A. The Rietveld Method. 1st Ed. Oxford University Press, Oxford, (UK), 1992, p. 167–185.

[15] H.M. Rietveld, Journal of Applied Crystallography, 2 (2) (1969) 65–71.

[16] R.A. Young, Introduction to the Rietveld Method. In: Young, R. A. The Rietveld Method. 1st Ed. Oxford University Press, Oxford (UK), 1992, p. 1–38.

[17] M. Leikola, Solid-State Reduction of Chromite with Methane and Hydrogen. Master's Thesis, Aalto University, School of Chemical Technology, Espoo, 2015.

[18] Handbook of Chemistry and Physics, 56th Edition. CRC Press, Cleveland (OH), 1975.

ODREĐIVANJE STEPENA METALIZACIJE KOD PRETHODNO REDUKOVANOG HROMITA PUTEM ANALIZE SLIKE I RIETVELDOVE ANALIZE

T. Leino [a], P. Taskinen [a,*], R. H. Eric [a, b]

[*a] Departman za hemijsko i metalurško inženjerstvo, Alto univerzitet, Alto, Finska
[b] Fakultet za hemijsko i metalurško inženjerstvo, Univerzitet u Vitvatersrandu, Južna Afrika

Apstrakt

Stepen metalizacije kod uzoraka prethodno redukovanog hromita je određen pomoću dve metode. Uzorci hromita su redukovani u čvrstom stanju u prisustvu smeše gasova koja je sadržala metan i vodonik. Prva metoda je bila analiza slike mikrografskih oblika dobijenih skenirajućim elektronskim mikroskopom, gde su faze teških metala predstavljene kao jarko bele površine koje je lako segmentovati pomoću algoritma za segmentaciju slike. Druga upotrebljena tehnika je bila Rietveldova analiza oblika dobijenog rendgenskom difrakcijom praha koji se uklapa sa izračunatim profilom na dijagramu za oblike dobijene rendgenskom difrakcijom da bi se dobila informacija o kvantitetu faza. Rietveldova metoda i analiza kompozicije faza su izvršene u programu PANalytical's X'Pert HighScore Plus na osnovu XRPD (rendgenska difrakcija praha) podataka. Rezultati dobijeni korišćenjem obe metode su se dobro slagali. Stepen metalizacije za ispitane uzorke se kretao od 15 do 65% u zavisnosti od stepena redukcije koji je zavisio od funkcije vremena, temperature redukcije i sadržaja metana u smeši gasova. Dobijeni rezultati obećavaju i pokazuju da se i analiza slike i Rietveldova analiza mogu koristiti kao metoda za brzo određivanje stepena matalizacije kod prethodno redukovanih uzoraka u poređenju sa sporom i zamornom hemijskom analizom.

Ključne reči: *Gvožđe hromit, Metalizacija, Analiza slike, Rietveldova analiza.*